Combustion and Flame 161 (2014) 1408–1416

Contents lists available at ScienceDirect

Combustion and Flame

journal homepage: www.elsevier.com/locate/combustflame

Do nanoenergetic particles remain nano-sized during combustion?

Purnendu Chakraborty, Michael R. Zachariah *

University of Maryland, College Park, MD, United States

ARTICLE INFO

Article history:
Received 21 November 2011
Received in revised form 25 January 2013
Accepted 18 October 2013
Available online 18 February 2014

Keywords:
Nanoparticles
Metals burning
Molecular dynamics
Sintering

ABSTRACT

It is axiomatic that the burning time dependence on particle size follows an integer power law dependence. However, a considerable body of experimental data show a power dependence less than unity. In this paper, we focus on what might be responsible for the fractional power dependence observed for the burning time for nanoparticles (e.g. Al and B). Specifically we employ reactive molecular dynamics simulations of oxide-coated aluminum nanoparticles (Al-NPs). Since most nanomaterials experimentally investigated are aggregates, we study the behavior of the simplest aggregate – a doublet of two spheres. The thermo-mechanical response of an oxide coated Al-NP is found to be very different than its solid alumina counterpart, and in particular we find that the penetration of the core aluminum cations into the shell significantly softens it, resulting in sintering well below the melting point of pure alumina. For such coated nanoparticles, we find a strong induced electric field exists at the core–shell interface. With heating, as the core melts, this electric field drives the core Al cations into the shell. The shell, now a sub-oxide of aluminum, melts at a temperature that is lower than the melting point of aluminum oxide. Following melting, the forces of surface tension drive two adjacent particles to fuse. *The characteristic sintering time (heating time + fusion time) is seen to be comparable to the characteristic reaction time, and thus it is quite possible for nanoparticle aggregates to sinter into structures with larger length scales, before the bulk of the combustion can take place.* This calls into question what the appropriate 'effective size' of nanoparticle aggregates is.

1. Introduction

Aluminum nanoparticles (Al-NPs) are the subject of considerable research in energetic materials due to their high energy density, low cost, and high reactivity. Two particular applications relevant are the addition of Al-NPs to high explosives to boost the energy density, and the use of Al-NPs as a fuel in binary thermite systems. In either case the use of nanometric scale particles is primarily to increase reactivity by reducing the characteristic mass transport length scales. In both applications, the particles are subjected to very intense heating, a fact that complicates experimental investigations. On exposure to air, aluminum particles form a native oxide (Al_2O_3) coating. This shell is typically uniform and amorphous, with a thickness of 2–5 nm [1]. While micron-sized aluminum particles have been reported to have an ignition temperature that is very close to the melting point of the oxide shell (~2300 K), Al-NPs have experimentally been observed to ignite closer to the melting temperature of Al (~930 K). Thus understanding the interaction of the low melting aluminum core with the high melting Al_2O_3 shell during rapid heating is critical in understanding the ignition mechanism of Al-NP's. At present there are two non-complementary explanations for the ignition mechanism of Al-NPs subjected to rapid heating are:

a. Melt dispersion mechanism – under high heating rate, the aluminum core melts and expands in volume, exerting high stress on the solid shell. If high enough, the stress causes the oxide shell to rupture, and tensile forces subsequently unload the aluminum as small molten clusters at high velocities [2].
b. Diffusion mechanism – the shell undergoes some transition, i.e. physical cracking or polymorphic phase transitions, allowing aluminum to diffuse through the shell. The mass transport is governed by an effective diffusion coefficient of the aluminum through the permeable shell [3].

The exact physical mechanism for this ignition phenomenon is currently unclear, and this is largely due to the lack of experimental techniques. This paper however will not deal directly deal with this debate, but consider the rather curious behavior observed in the scaling laws for burning, as particle size gets smaller.

* Corresponding author. Fax: +1 301 314 947.
E-mail address: mrz@umd.edu (M.R. Zachariah).

http://dx.doi.org/10.1016/j.combustflame.2013.10.017
0010-2180/

In studies on the combustion characteristic of boron nanoparticles [4], the particle size dependence of burning time (t_b) is found to decrease as the particle size decreases into the nanometer range. The burning times of larger particles, 30–100 μm [5,6], have long been known to be consistent with the d^2-law (diffusion-limited burning). A transition from diffusion-controlled to a kinetically-controlled is seen to occur at particle sizes of ~10 μm. However below ~10 μm particles burning time which should be expected to roughly scale as $\sim d^1$ (kinetic limited regime) [7–9] actually are seen to demonstrate dependencies less than unity; see Fig. 6 of [10]. As has been pointed out [10], the exact exponent cannot be determined due to uncertainty in the size distribution and particle agglomeration. Nevertheless, given the significant deviations from integer dependencies, it is also possible that other physical characteristics are at play not captured in a shrinking–core model. The size dependence further reduces to $\sim d^{<0.5}$ for sub-micron particles, see Fig. 17f [4]. Thus there is "apparently" only minimal gain in reducing particle size in the sub-micron range/nanoscale. Nano-Aluminum also exhibits a similar size independence in the nanoscale regime with $t_b \sim d^{0.3}$ [11]. While more data is needed in the small size regime, in general we can conceptually summarize the experimental data in Fig. 1. This leaves open an explanation of this behavior.

Much of what is known about how super-micron particles burn is through direct imaging. But while burning can be directly imaged for large particles, nanoparticles pose a particularly challenging experimental problem. It is difficult to design experiments mimicking both the rapid heating, speculated to be around 10^8 K/s [12], and observe the physical changes occurring. A few experimental studies have recently emerged [3,13], to directly observe reaction on time scales relevant to combustion. In a recent work [13], a mixture of Al-NPs/WO_3 (fuel/oxidizer) was imaged in a high resolution Scanning Electron Microscope (SEM). The images before and after heating are shown in Fig. 2.

In the region of proximity of the fuel (Al) and oxidizer (WO_3), significant changes are seen (bulk of WO_3 does not melt and remains unchanged). It is argued that the Al and WO_3 come into surface contact and react at the interface. The heat generated melts adjacent particles leading to sintering. Chung et al. [14] modeled the oxidation enthalpy of Al-NPs as a function of the Al-NP size. They found the reaction enthalpy of Al-NP (aggregated) → bulk-Al_2O_3 to increase with decreasing particle size. The increased energy released with decreasing primary size would lead to faster sintering of the aggregates into bulk alumina. The results raise strong questions about the "effective" particle size and how it would impact reactivity, since large amounts of sintering serves to completely change the size and morphology of the particles. This is important since nanoparticles are mostly agglomerated.

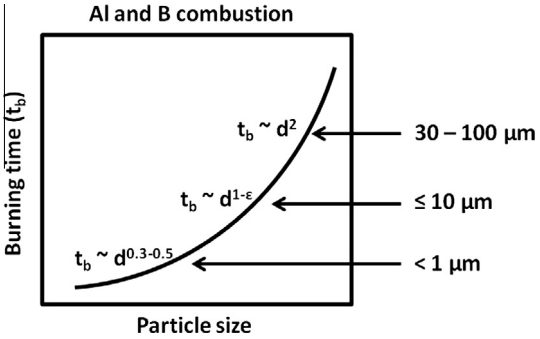

Fig. 1. Conceptual figure showing experimentally determined diameter dependence on burning time.

One possible explanation then for the low size dependence of burning times for nanoparticles, seen conceptually in Fig. 1, is that nanoparticles, when heated, cease to exist as single primary particles, and instead sinter to form structures with characteristically larger length scales. The goal of this work is to investigate the thermal response of oxide coated aluminum nanoparticles using molecular dynamics simulation to address the question of the likelihood of nanoaluminum sintering on a time scale commensurate with the characteristic reaction time. The relevant question, applicable for both Al-NPs in a high explosive and binary thermites, is whether nanoparticles sinter into characteristically larger structures well before the bulk of reaction can take place? On the basis of this work, the answer appears to be yes.

2. Simulation details

Molecular Dynamics (MD) methods are ideally suited to study such a problem because of the small particle sizes being considered and the lack of physical property data to implement a phenomenological model. We employed the ReaxFF (reactive) potential [15] to describe the interactions between the atoms which has been shown to accurately predict the dynamical and reactive processes of aluminum/aluminum oxide systems [16]. In contrast to traditional empirical potentials, the reactive potentials have the advantage of being able to simulate bond breaking, bond formation and charge transfer, and thus off-stoichiometry cation–anion interactions. The force field parameters for Al/Al_2O_3 system was developed and optimized using the results of first principles calculations. The charges of Al and O in α-Al_2O_3 were found to be in good agreement with Quantum Mechanical (QM) results. The authors studied solid-Al/α-Al_2O_3 interface and found it to be sharp with an equilibrium separation that agreed well with density functional theory (DFT).

However, the advantages offered by ReaxFF, also result in at least an order of magnitude more expensive than traditional MD simulations in addition to a significantly larger memory requirement. The ReaxFF potential has been integrated into the large scale parallel MD software Lammps [17] which has been used for the present study. The MD simulations were carried out on the TACC Ranger system as part of the TeraGrid network, using 8–128 processor cores. The equations of motion were integrated using the Verlet algorithm employing a time-step of 1 fs. Temperature was controlled by rescaling the velocities to the desired temperature at every time-step if the difference between the target and desired temperature exceeded 10 K.

Here we studied two different particle sizes (8 and 16 nm in diameter) – the smaller 8 nm particle consists of an ~5 nm diameter aluminum core coated with an ~1.5 nm oxide shell. A pure Al particle was first created from an *fcc* crystal by considering only the atoms within a 2.5 nm radius. It was subsequently equilibrated at 300 K. Following equilibration, the Al particle was coated with a crystalline Al_2O_3 shell. The coated particle was then heated to 500 K and the temperature maintained at 500 K for equilibration. A true equilibrium was, however, never reached – due to a (very) slow continuous diffusion of core Al atoms into the shell resulting in a continually decreasing potential energy profile. The diffusion being slow at 500 K, a configuration obtained after 1 ns of equilibrations was taken as the (pseudo) equilibrated structure. For comparison purposes a pure oxide particle of diameter 8 nm was built as well. The larger, 16 nm, particle, built similarly, consists of an ~12 nm core aluminum coated with an ~2 nm oxide shell (a total of ~200,000 atoms).

Three simulations were carried out using each of these particles. The system consisted of a particle and its translated image placed adjacent to each other, with the minimum distance

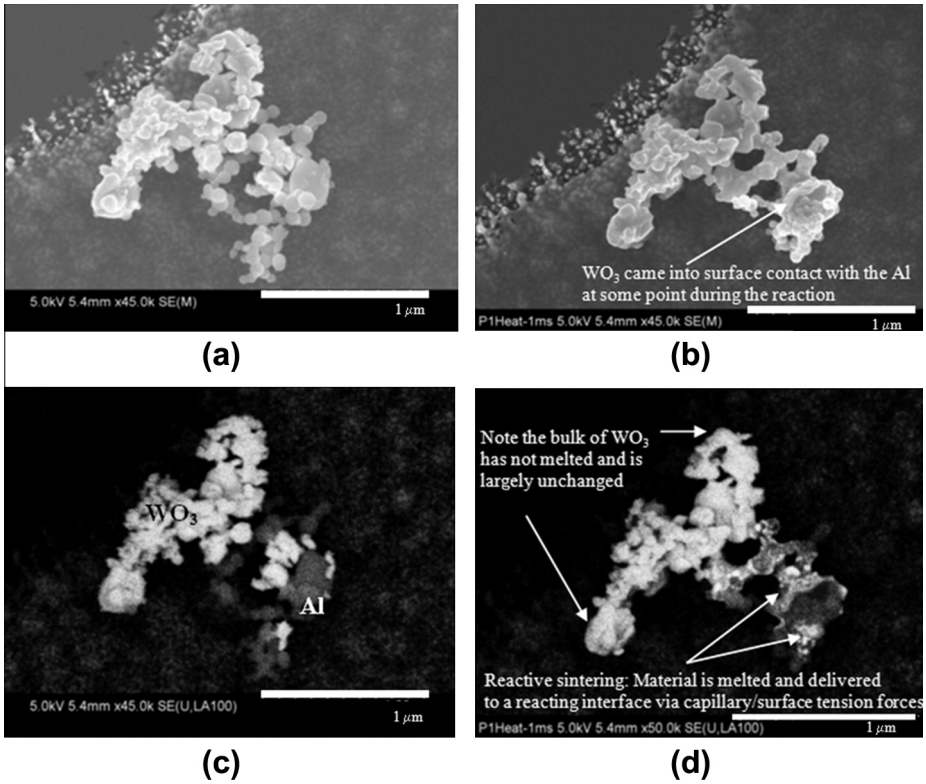

Fig. 2. SEM images of Al-NPs/**WO_3** (a) before and (b) after heating to 1473 K at $\sim 10^6$ K/s. (c) and (d) panels are the respective backscattered electron (BSE) images: the bright particles are W/**WO_3**, the darker particles are Al/Al_2O_3. Figure taken from [13].

between the surfaces being ~2–3 Å. This system was then enclosed in a box and heated rapidly at the rate of 10^{13}–10^{14} K/s: from 500 K to 2000 K. Obviously this heating rate is considerably faster than that experienced in a real combustion event. We are however constrained by the total time, of the order of nanoseconds, that can be realistically simulated in a molecular dynamics simulation. Using a parametric study, Puri et al. [18] found that a heating rate in the range 10^{13}–10^{14} K/s is sufficient to equilibrate particles as well as to resolve calculated thermodynamic and structural properties. The final temperature was intentionally kept below the bulk melting point of alumina (~2400 K). Subsequently, the system temperature was held at 2000 K.

3. Results and discussion

To evaluate the sintering and combustion times we begin by simulating the sintering of oxide coated aluminum. Two small (8 nm) coated particles, equilibrated at 500 K, are placed adjacent to each other and heated rapidly at the rate of 10^{14} K/s (total time of 15 ps). The temperature is then held at 2000 K for another 1 ns. To compute the timescale for sintering, the normalized moment of inertia (MOI) is tracked throughout the simulation. The normalized MOI converges to unity when the two particles have fused completely to form a sphere. Figure 3 plots the normalized MOI along with cross-sectional views of six temporal snapshots of the simulation. Snapshots at 0 and 15 ps are for the configurations before and after heating. Heating causes the particles to undergo a volumetric expansion with melting of the core aluminum. Since the coefficient of thermal expansion of aluminum is considerably greater than that of alumina (linear coefficient of aluminum being approximately four times that of alumina), one would expect the core pressure to increase significantly, possibly leading to rupturing of the shell. However no mechanical failure was observed. The core Al atoms, were instead seen to diffuse into the oxide shell with the shell becoming richer in aluminum. The shell Al and O atoms on the other hand diffused inwards leading to a more homogeneous overall composition than the original core–shell structure.

The remaining snapshots show that after the inter-diffusion of core Al into the shell, fusion between particles begins and continues. The sintering time, time to heat the particles, plus the time to fuse completely, can be read off directly from the normalized MOI curve to be ≈0.7 ns. The important point here is that the 2 coated Al-NPs, heated to 2000 K, sinter completely despite that fact that the final temperature is held some ~400 K below the melting temperature of alumina. However, at the onset of sintering (~100 ps) it would be incorrect to consider the shell as alumina. The shell is clearly a sub-oxide of aluminum and is expected to have very different thermo-mechanical properties. In other words, very rapidly the shell is no longer alumina, and any phenomenological based model that uses the properties of alumina, even if there were in principle applicable to these length scales, would be in significant error.

To demonstrate this point more rigorously, an identical temperature-ramp simulation was conducted with two 8 nm oxide (alumina) particles. Figure 4 shows that even though the particles show thermal expansion effects, and form a covalent bridge, no significant neck growth can be observed. This would seem to confirm that core–shell aluminum–alumina particles would sinter well below the bulk melting point of alumina, due to the internal core-to-shell diffusion of aluminum ions.

To study the structural differences between the pure oxide, and the coated particles, the Al–O atom radial distribution function, $g(r)$, was computed. $g(r)$ gives the local atomic arrangement and is a tool to distinguish between solids and liquids. While crystalline solids are characterized by a repeating sequence of sharp peaks (indicating long-range order) separated by distances between

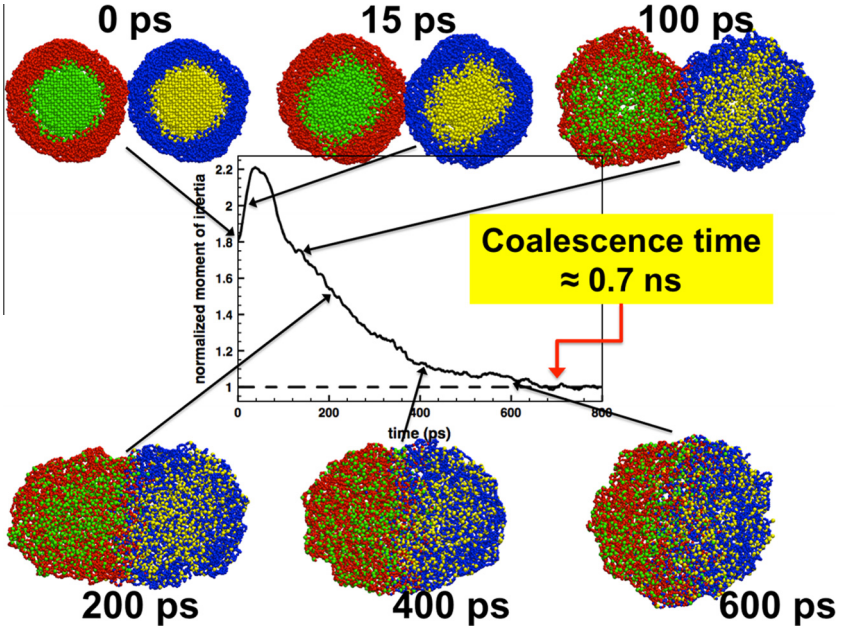

Fig. 3. Sintering of two 8 nm aluminum particles with oxide shell – (a) initial configuration and (b) system at the end of rapid heating. Panels (c)–(f) represent subsequent configurations when the temperature is held at 2000 K. Colors: blue and red represent the shell (oxide) atoms whereas yellow and green represent the core (aluminum) atoms. (For interpretation of the references to color in this figure legend, the reader is referred to the web version of this article.)

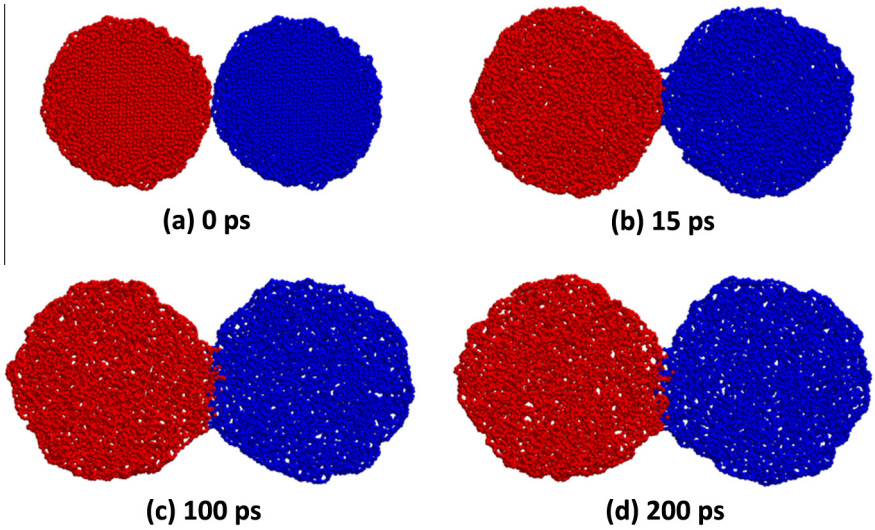

Fig. 4. Simulation of a system consisting of two alumina particles. i.e. no sintering in the case of alumina. Temperature ramp is identical to the case depicted in Fig. 3.

neighbors, $g(r)$ for liquids has few peaks at short distances and no long range order. The radial distribution functions for the coated and oxide particles at 200 ps are plotted in Fig. 5. The sharp peak and practically no long-range order in the case of the oxide particle indicate that the oxide particle is an amorphous solid. The Al–O radial distribution function for the coated particle, on the other hand, exhibits the shape typically found for liquids – diffused peak (with fewer nearest neighbors) and no long-range order – indicating that the shell has melted and is in the liquid state. Thus, while the oxide particles remain solid at 2000 K, the coated particle is in a molten or near molten state, such that the forces of surface tension can drive the fusion.

To explore the sintering behavior in more detail a third sintering simulation was carried out with two larger (16 nm) coated particles placed adjacent to each other and heated at the rate of 10^{13} K/s (over a period of 150 ps) – an order of magnitude slower than the case with smaller particles. In the following, structural changes due to heating and its effects on the induced electric field/mass transfer are probed for this larger (16 nm) particle followed by a comparison of sintering and reaction timescales.

3.1. Radial atomic density

Figure 6 shows the radial density at different times, indicating were each atom type is as a function of time. Radial density [19] was calculated by considering concentric spherical shells centered at the center-of-mass of the particle. The density at a distance r from the center-of-mass was then computed as the total mass inside the shell at distance r divided by the shell volume. Averaging over snapshots over 40 ps of simulation time resulted in the density plots.

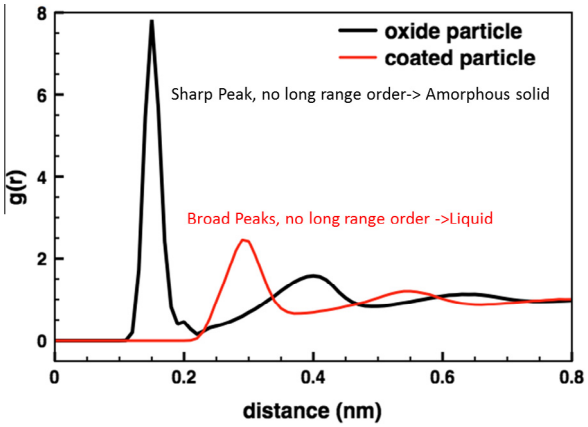

Fig. 5. Al–O atomic radial distribution functions for oxide coated nanoaluminum and aluminum oxide particles at 200 ps.

Initially at 500 K, (a) the particle exhibits a core–shell structure defined by a clear interface at ~60 Å. The core Al had a density of 2.7 g/cc, consistent with the bulk density of solid Al. The shell, however, expanded in volume to a density of 3.1 g/cc from the prescribed initial density of 4.0 g/cc. It is interesting to note some diffusion of core Al atoms into the shell. As mentioned earlier, this diffusion is an ongoing process, much slower at lower temperature and speeding up with the melting of the Al core. As a result of heating and (b) the core melts, as is evidenced by a reduced density (2.0 g/cc). With the core Al becoming more mobile, significantly more core Al atoms diffuse into the shell – panels (b) and (c) – along with diffusion of shell atoms (both Al and O) inwards. The shell can no longer be considered to be pure alumina. Instead the shell becomes aluminum rich forming a sub-oxide. As the temperature is held constant at 2000 K, the pure aluminum core shrinks along with an inwards expansion of the increasingly aluminum-rich shell. Finally, a near homogeneous distribution of species in the particle is obtained – panel (d).

3.2. Induced electric field driving transport

In a recent work on core–shell particles [20], the radial diffusivity of the core Al atoms was computed at different temperatures and compared with the overall diffusivity. It was found that an 'induced electric field' (rather than Fickian diffusion) drives the diffusion of core Al into the shell. The idea that oxidation growth occurs through the 'migration of charged species' was first proposed by Carl Wagner in 1933 [21]. In 1948, the Cabrera-Mott model [22] was developed that described the growth of thin oxide films on metal crystals driven by an induced electric field that causes metal ions to migrate to the surface. More recently a modified form of the Cabrera-Mott model was applied to nanometer-sized particles [23]. The induced electric field was found to be much stronger in such small particles compared to a flat surface, thereby increasing the oxidation rate significantly. Dreizin et al. [24] further modified this model to account for volume changes in the shrinking core and expanding shell.

Figure 7 plots the radial charge density before and after heating. The plots are obtained by averaging over 40 ps of simulation time. The positively charged core, coupled with a negatively charged shell (in the initial configuration, both the core and shell were charge neutral) results in an electric field induced in the particle, most prominently at the core–shell interface.

The electric field at each ion of the particle was then computed directly using Coulomb's law by summing over contributions from all neighboring atoms at a distance greater than 0.15 nm – to exclude the effect of the covalently bonded ions (the nearest neighbor peak in the radial distribution function for the covalently bonded shell atoms occurred at 0.15 nm). Figure 8 shows the radial component of the electric field (along with the density profile for comparison) in the particle at various times. A positive value indicates a radially outwards electric field. Thus the core Al atoms in the interfacial region are under a radially outward electric field. Figure 8a shows the electric field profile for the particle at 500 K – before heating. This electric field at the interface accounts for the slow continuous diffusion of core Al atoms into the shell despite the fact the core has not melted and is not under enhanced pressure. Figure 8b represents the field at 2000 K, at the end of heating. With time, the electric field moves inwards along with the core–shell interface and dissipates, Fig. 8c and d. Also note that the electric field changes sign across the thickness of the shell region. This is clearly visualized by plotting the electrical force on the O atoms. Similar to the electric field calculations, the electrical force on O atoms was computed using Coulomb's Law by summing over contributions from all neighboring atoms excluding the bonded atoms. Figure 9 shows the direction of the electrical force on the oxygen atoms. As indicated by the changing sign of the electrical field, the O atoms closer to the interface experience an inward electrical force while the O atoms near the particle surface experience an outward electrical force. This is a probable explanation for the initial expansion of the shell during equilibration of the particle at 500 K.

3.3. Mass transport within a particle

Henz et al. [20] showed that at 2000 K, almost all (>99%) of the core Al atom flux is due to the induced electric field, with the remainder due to concentration and pressure gradients. They estimated the flux of the core Al atoms using the Nernst-Planck equation [25] to be $\sim 31 \frac{\text{mol}}{\text{cm}^2\ \text{s}}$. In this work, we compute the flux directly. The flux at time t_i across a sphere of radius r, centered at the center of mass of the particle, is calculated as

$$J(r, t_i) = \frac{N(t_{i-1}) - N(t_i)}{4\pi r^2 (t_i - t_{i-1})} \tag{1}$$

where $N(t)$ is the number of atoms, of a particular species, inside a sphere of radius r at time t. By construction, a positive value of the flux indicates an outward motion of atoms. Averaging over a period of 40 ps, the flux of core Al and shell O ions, for different times is plotted in Fig. 10. During the period of heating (0–150 ps), the flux of core Al atoms at the interface increases from a nearly zero net flux to a value of $\sim 38 \frac{\text{mol}}{\text{cm}^2\ \text{s}}$. This value is consistent with the previously estimated value.

Using the collision frequency for oxygen molecules in the gas phase, we estimate the flux of oxygen molecules hitting the particle surface to be $\sim 1 \frac{\text{mol}}{\text{cm}^2\ \text{s}}$. *Thus the outward flux of aluminum though the shell is considerably faster than the reaction rate with the surface. As a result the surface will become Al rich and some evaporation will take place.* In a prior work [26], we have found some conditions experimentally, in which an Al-NP oxidation results in a hollow product particle consistent with the above analysis. During the period when the temperature is held constant the peak of the flux plot shifts inwards as the core shrinks and finally reaches nearly zero net flux – consistent with the electric field results discussed earlier. The important point here is that a strong electric field is induced at the core–shell interface due to the positively charged core and the negatively charged shell. This electric field, in turn, causes migration of ions finally forming a homogeneous sub-oxide of Al. The idea that the flux of the ions is governed by the induced electric field is also strongly supported by the transport of oxygen anions. Comparing the region between 8 and 10 nm at 150 ps, we see an outward flux of oxygen anions, which is consistent with an

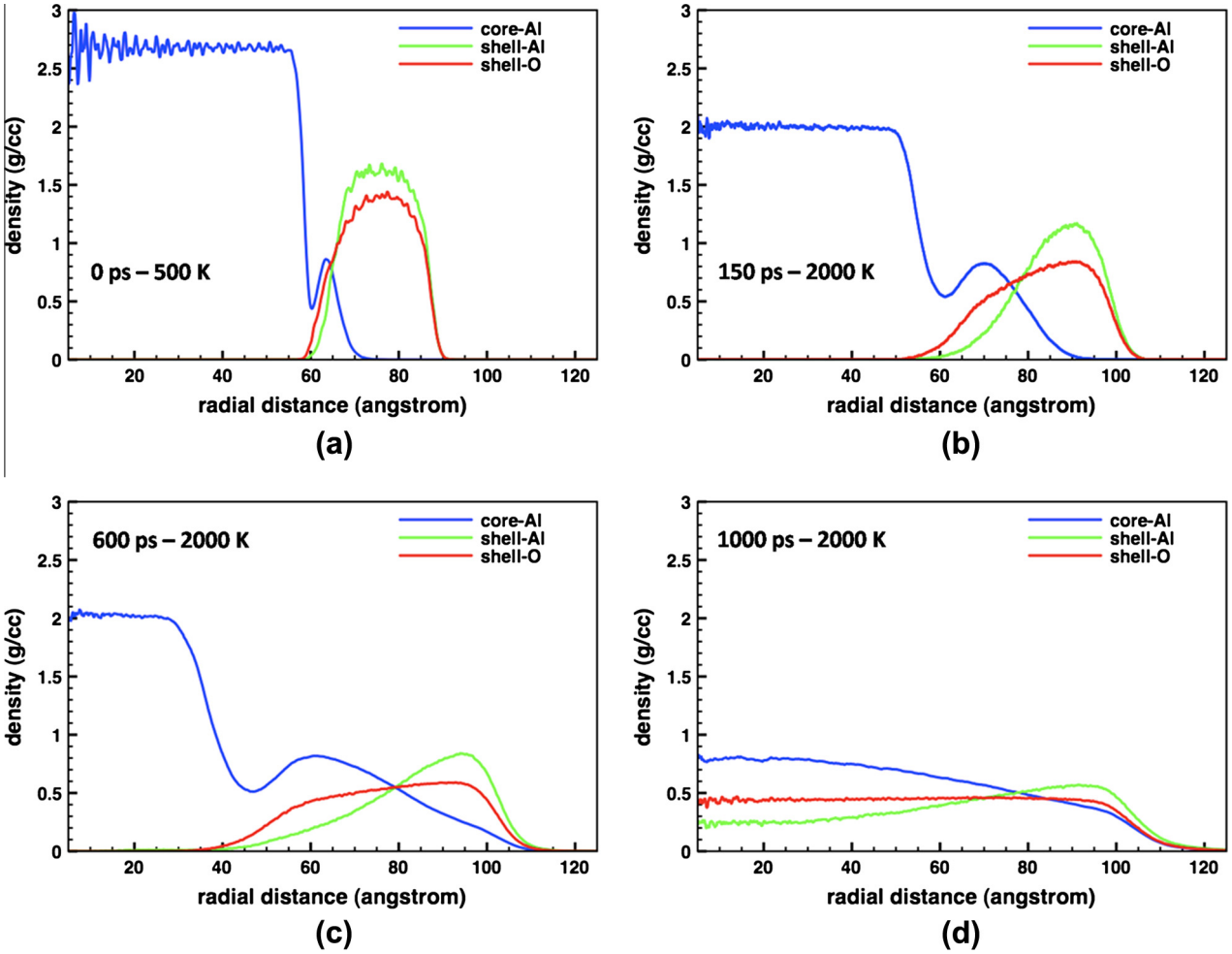

Fig. 6. Radial density plots at different times, shows movement of Al and O ions.

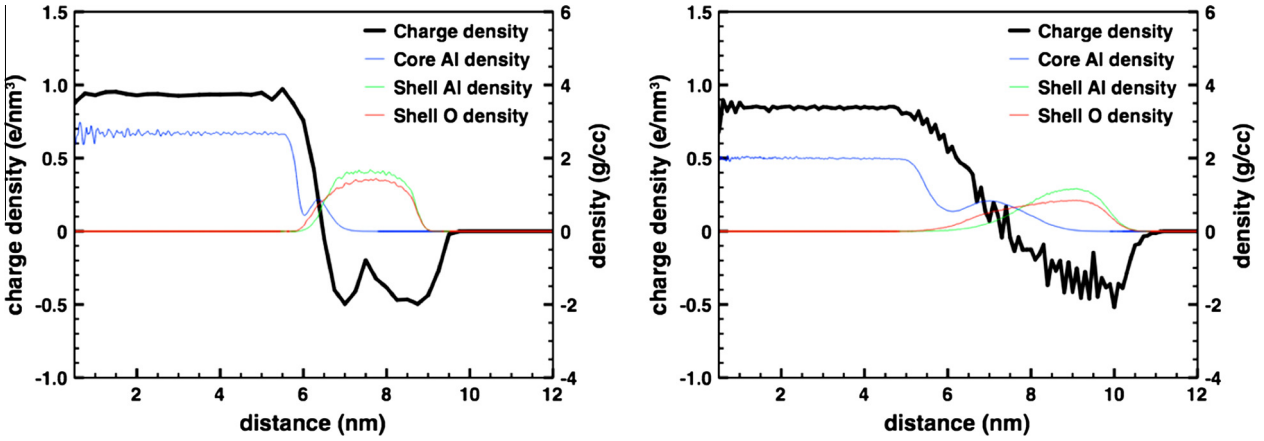

Fig. 7. Charge density in the left particle in aggregate before and after heating. For comparison, the density plot is also included.

inward electric field. Subsequently, with the core–shell interface moving inwards, at 700 ps, a radially outward electric field in the region 2–5 nm drives the oxygen anions inwards. The induced electric field thus drives the original core–shell particle towards a more uniform particle through migration of ions in the particle.

The formation of hollow particles was also seen in this work as a transient state as a gap between the core and the shell regions of the particle and can be attributed to the higher outward diffusion of Al ions compared to the inward diffusion of the shell ions. For example, at 300 ps, in the region between radii 4 nm and 5 nm, the outward flux of ~27 $\frac{\text{mol}}{\text{cm}^2\,\text{s}}$ of core Al cations is almost double that of the inward flux ~14 $\frac{\text{mol}}{\text{cm}^2\,\text{s}}$ of the shell O anions. This difference in fluxes leads to a transient hollow structure, prominently visible in 11. The 'gap' between the core and the shell vanishes with transition towards the more homogeneous particle.

3.4. Characteristic times: sintering Vs reaction

The snapshots of the sintering simulation of the larger 16 nm particles are presented in Fig. 11. In these simulations, the final

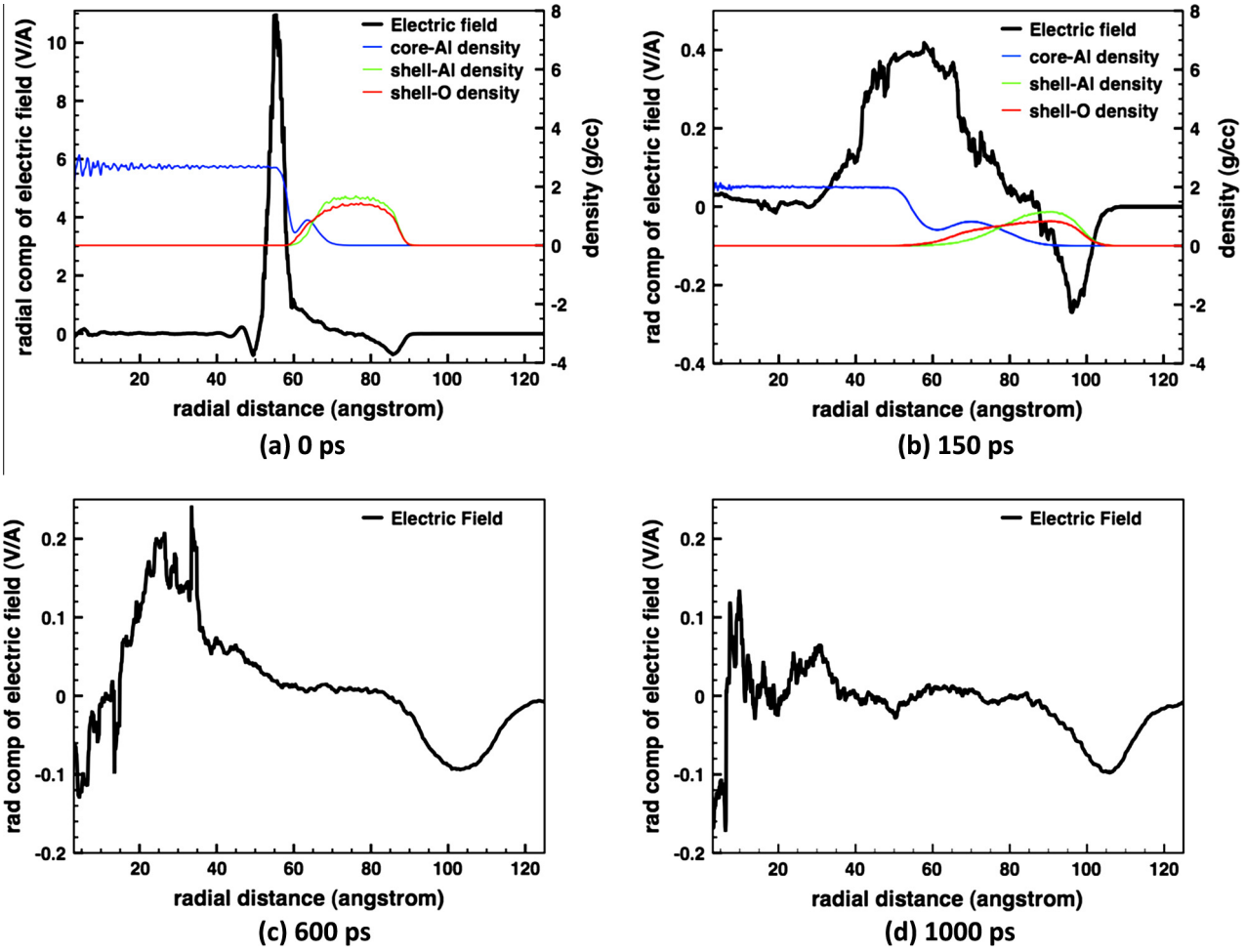

Fig. 8. Radial component of the induced electric field (volt/Angstrom) acting on the particle. With time, the peak of the electric field moves inwards and dissipates.

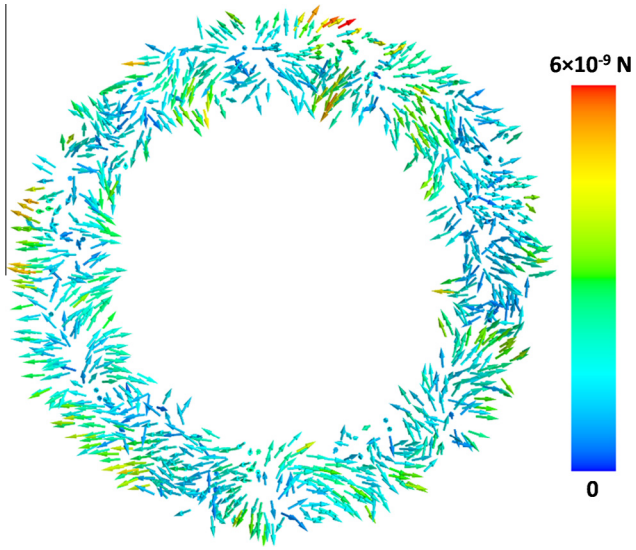

Fig. 9. Electrical force on O atoms in the shell at 500 K. O atoms closer to the core experience an inward electric force, while O atoms near the surface experience an outward electric force.

temperature was fixed at 2000 K. Similar behavior (inter-diffusion followed by fusion) is expected as long the final temperature is greater than the melting point of the aluminum (core). As discussed earlier, the particle size dependence of burning time for Al and B particles was seen to decrease with diminishing particle size into the nanometer range (Fig. 1). The diffusion and kinetic limited burning theories generally apply to single particles or droplets. Nanoparticles, on the other hand typically exist as aggregates (for commercially available nanoparticles, the specified size is the average of the primary sizes in the aggregates). The important question here is what is the characteristic time scale for sintering relative to reaction. The sintering timescale is important since this would determine the effective particle size undergoing combustion. If the timescale for sintering is faster or at least comparable to the reaction timescale (combustion of the bulk of the nanoparticles), the burning time would then correspond to that of particles with larger characteristic length scales.

Reaction times are strongly dependent on the particular combustion system and configuration. Using a combustion cell, the pressure rise time for Al based thermites was seen to be of the order of 10 μs [27]. Al nanoparticle combustion behind reflected shock waves in a shock tube at elevated pressures and temperatures yielded a reaction time of 50–500 μs [28]. For the purpose of comparison, we take 10 μs as the characteristic reaction timescale as the most conservative case.

The sintering time, is a sum of two components – time to heat the particles from the ambient temperature to the final temperature, and the fusion time. Since the coated particles are in the liquid state, the fusion takes place through viscous flow and the characteristic fusion time can be computed using Frenkel law [29] as

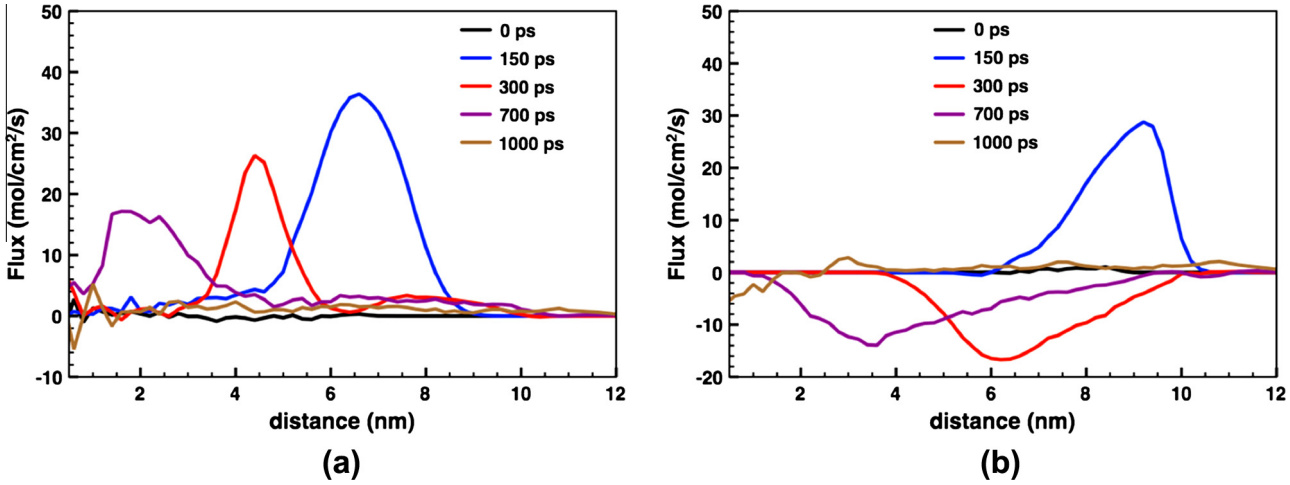

Fig. 10. Flux across the oxide coated Al particle – of (a) core Al and (b) shell O – at various times. A positive flux is radially outward.

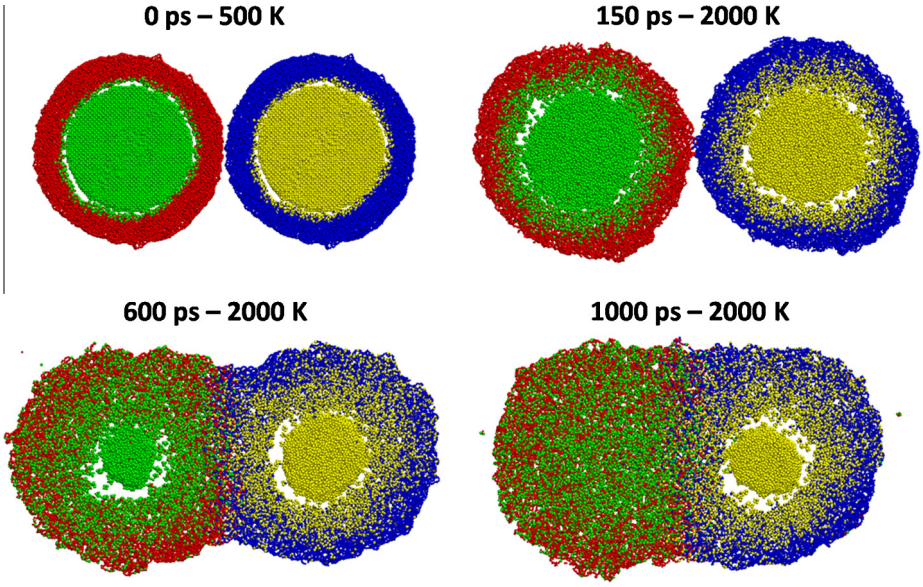

Fig. 11. Sintering simulation snapshots of the 16 nm oxide coated Al particles.

$$\tau_F = \frac{\eta d_p}{\sigma} \tag{2}$$

where η is the temperature-dependent viscosity, d_p is the particle diameter and σ is the surface tension. If surface tension at these length scales can be assumed to be size-independent, the ratio of the fusion times of two different sized particles would be equal to the ratio of their diameters. Since our calculations show that two 8 nm particles completely fuse in ≈0.7 ns, we can, by scaling arguments, estimate the fusion time for two 50 nm particles to be ≈5 ns. Real aggregates have more than two primary particles, which can be accounted for by using Hawa & Zachariah's [30] power law modification to Frenkel's law. For N primaries of equivalent size in an aggregate of fractal dimension D_f, the fusion time is given by

$$\tau = \frac{\eta d_p}{\sigma}(N-1)^{0.68^{D_f}} \tag{3}$$

Transmission Electron Microscope (TEM) images show that the fractal dimension of vapor grown aggregates is typically ≈1.8. So even for an aggregate consisting of 100 nanoparticles with average primary size of 50 nm, the total fusion time, calculated using Eq. (3), would be ≈50 ns. In our simulations, for computational efficiency, the heating rate was considered to be much larger than the speculated rate of 10^8 K/s. According to the experimental heating rate, the time to heat the particles from 500 K to 2000 K would be ≈15 μs This heating time, being several orders of magnitude larger than the fusion time, is thus the effective sintering time.

Thus the sintering time is competitive with the reaction time. i.e. Al-NPs should sinter into larger structures before a significant amount of combustion can take place. Depending on the number of primaries in an aggregate, the equivalent sphere may not be nano-sized and as such, there may not be an advantage in using (aggregated) nanoparticles under some critical size as energetic materials, since the main advantage of the nanoparticles, the high surface area to volume ratio, is negated.

4. Conclusion

Reactive Molecular Dynamics simulations were carried out to study if the lower power dependence on particle size for burning nanoscale materials, was caused by particle sintering. Rapid heating of aluminum core/oxide shell particles found that as the

core melts, the core Al atoms diffuse radically outward into the oxide shell, driven by an induced built-in electric field.

With the diffusion of core Al cations into the shell, the shell, which is now a sub-oxide of aluminum, melts at temperatures considerably lower than the melting point of the oxide. Forces of surface tension then drive fusion of two such liquid particles. As a result, for aggregates of nanoparticles, sintering into larger structures can occur on the same time scale as combustion. This qualitatively may explain why the burning times do not get significantly shorter for very small particles.

Acknowledgments

This research was supported by the Army Research Office and the National Science Foundation through TeraGrid resources provided by TACC under grant number TG-DMS110011. The authors would also like to thank Prof's Nick Glumac and Edward Dreizin for helpful discussion on the power dependence on particle burning.

References

[1] M. Trunov, M. Schoenitz, E. Dreizin, Combust. Theor. Model. 10 (4) (2006) 603–623, http://dx.doi.org/10.1080/13647830600578506.
[2] V. Levitas, B. Asay, S. Son, M. Pantoya, Appl. Phys. Lett. – ARTN 071909 DOI 10.1063/1.2335362, 2006.
[3] S. Chowdhury, K. Sullivan, N. Piekiel, L. Zhou, M. Zachariah, J. Phys. Chem. C (2010) 9191–9195, http://dx.doi.org/10.1021/jp906613p.
[4] G. Young, K. Sullivan, M. Zachariah, K. Yu, Combust. Flame 156 (2) (2009) 322–333, http://dx.doi.org/10.1016/j.combustflame.2008.10.007.
[5] A. Macek, J.M. Semple, Combust. Sci. Technol. 1 (1969) 181–191.
[6] A. Maček, Symp. (Int.) Combust. 14 (1) (1973) 1401–1411. 10.1016/s0082-0784(73)80125-0.
[7] S.C. Li, F.A. Williams, Ignition and Combustion of Boron Particles (1993) 248–271.
[8] C. Yeh, K. Kuo, Prog. Energy Combust. Sci. 22 (6) (1996) 511–541.
[9] T. Bazyn, H. Krier, N. Glumac, Proc. Combust. Inst. 31 (2007) 2021–2028, http://dx.doi.org/10.1016/j.proci.2006.07.161|10.1016/j.proci.2006.07.161.
[10] R. Yetter, G. Risha, S. Son, Proc. Combust. Inst. 32 (2009) 1819–1838, http://dx.doi.org/10.1016/j.proci.2008.08.013|10.1016/j.proci.2008.08.013.
[11] Y. Huang, G. Risha, V. Yang, R. Yetter, Proc. Combust. Inst. 31 (2007) 2001–2009, http://dx.doi.org/10.1016/j.proci.2006.08.103.
[12] V. Levitas, Combust. Flame 156 (2) (2009) 543–546, http://dx.doi.org/10.1016/j.combustflame.2008.11.006.
[13] K.T. Sullivan, W.-A. Chiou, R. Fiore, M.R. Zachariah, Appl. Phys. Lett. 97 (13) (2010) 133104.
[14] S. Chung, E. Guliants, C. Bunker, P. Jelliss, S. Buckner, J. Phys. Chem. Solids 72 (6) (2011) 719–724, http://dx.doi.org/10.1016/j.jpcs.2011.02.021.
[15] A. van Duin, S. Dasgupta, F. Lorant, W. Goddard, J. Phys. Chem. A (2001) 9396–9409, http://dx.doi.org/10.1021/jp004368u.
[16] Q. Zhang, T. Cagin, A. van Duin, W. Goddard, Y. Qi, L. Hector, Phys. Rev. B (2004), http://dx.doi.org/10.1103/PhysRevB.69.045423 (ARTN 045423).
[17] S. Plimpton, J. Comput. Phys. 117 (1) (1995) 1–19.
[18] P. Puri, V. Yang, J. Nanopart. Res. 12 (8) (2010) 2989–3002, http://dx.doi.org/10.1007/s11051-010-9889-2.
[19] S.M. Thompson, K.E. Gubbins, J.P.R.B. Walton, R.A.R. Chantry, J.S. Rowlinson, J. Chem. Phys. 81 (1) (1984) 530–542.
[20] B. Henz, T. Hawa, M. Zachariah, J. Appl. Phys. (2010), http://dx.doi.org/10.1063/1.3247579.
[21] C. Wagner, Z. Phys. Chem. B (1933).
[22] N. Cabrera, N. Mott, Rep. Prog. Phys. (1948) 163–184.
[23] V. Zhdanov, B. Kasemo, Chem. Phys. Lett. (2008) 285–288, http://dx.doi.org/10.1016/j.cplett.2008.01.006.
[24] A. Ermoline, E. Dreizin, Chem. Phys. Lett. 505 (1–3) (2011) 47–50, http://dx.doi.org/10.1016/j.cplett.2011.02.022.
[25] Handbook of Electrochemistry, Elsevier, Amsterdam, 2007 (p.^pp).
[26] A. Rai, K. Park, L. Zhou, M. Zachariah, Combust. Theor. Model. 10 (5) (2006) 843–859, http://dx.doi.org/10.1080/13647830600800686.
[27] K. Sullivan, M. Zachariah, J. Propul. Power 26 (3) (2010) 467–472, http://dx.doi.org/10.2514/1.45834.
[28] T. Bazyn, H. Krier, N. Glumac, Combust. Flame 145 (4) (2006) 703–713, http://dx.doi.org/10.1016/j.combustflame.2005.12.017.
[29] S.K. Friedlander, Smoke Dust and Haze, Fundamentals of Aerosol Dynamics, Oxford University Press, 2000.
[30] T. Hawa, M. Zachariah, J. Aerosol Sci. 38 (8) (2007) 793–806, http://dx.doi.org/10.1016/j.jaerosci.2007.05.008.